NONLINEAR DYNAMICS IN OCEAN ENGINEERING

Edwin J. Kreuzer, Wolfgang M. Sichermann
Technical University Hamburg-Harburg
Mechanics and Ocean Engineering
[kreuzer, sichermann]@tu-harburg.de

Abstract The ability to predict and characterize the dynamic behavior of ocean engineering systems prior to financial commitments of their realization is an essential element of contemporary engineering. Linear models often do not provide sufficient accuracy and reliability to analyze and predict the dynamics of the real system in a satisfying manner. For example, ships in rough seas, moored offshore platforms and crane vessels under wave excitation show essentially nonlinear behavior. This paper illustrates how the methods of nonlinear dynamics can be employed for the prediction of operating limits and extreme responses of floating structures.

Keywords: Ship stability, mooring systems, floating cranes

1. Introduction

The international trade rests to a major extent on maritime traffic. The economic growth has led to the doubling of the global fleet size during the past three decades and, recently, to a rapid increase of the ship capacity. The marine exploitation of hydrocarbons and the power generation by offshore wind turbines assign further challenging tasks to ocean engineers. On the one hand, the design of mooring systems has to guarantee the safe positioning of drilling and production platforms in increasing water depths. And on the other hand, the development of offshore power plants in harsh environments, e.g. the North Sea, requires new approaches to the installation and maintenance procedures.

From statistical data we learn that at least one quarter of the total ship losses are caused by severe weather conditions. The current regulations and criteria for assuring the stability of a ship and preventing it from capsizing (the so-called prescriptive rules by the International Maritime Organization, IMO, 2002) are empirical and based on the properties of

the righting lever of the ship in still water. Model tests show, however, that the current stability criteria do not always correlate with the danger of capsizing. Hence, researchers agree that the actual criteria have to be modified. The IMO is working, therefore, on performance-based rules which apply to each specific ship.

Several computer programs have been developed for the numerical simulation of nonlinear ship motions in six degrees of freedom under the consideration of ship-wave interaction. Because of the complexity of the capsizing problem, these codes were used to evaluate statistical properties. The probability of capsizing was estimated, and heuristic arguments were used to interpret this probability and to derive stability criteria. Mathematically more advanced analysis techniques were recently applied to simple single-degree-of-freedom and regular wave excitation models and, with few exceptions, to more complicated models. By applying these techniques based on nonlinear dynamics theory it is possible to locate stability boundaries of the systems. The state of the art of (deterministic as well as stochastic) ship models has been very well documented in Spyrou and Thompson (2000).

For the accurate motion analysis of moored floating structures it is inevitable to account properly for the dynamic behavior of the attached mooring lines. Common practice is to use rather simple models based on a quasi-static approximation for the mooring systems to describe the interaction between the motion of structures and the restoring forces. These simplified models disregard the dynamics of the mooring line including the interaction between the fluid, the sea floor and the lines. For lines in deep water, these effects may cause a tremendous increase in the tensile force which cannot be predicted by simplified models.

We begin with the general formulation of the equations of motion for a floating body. Then, a basic model is derived for investigation of the large amplitude ship roll motions and capsizing in head and following seas. Next, we address crucial points for the dynamical modeling of mooring systems. The dynamical investigation of a floating crane serves as an example how analytical and numerical analysis techniques can be employed together successfully.

2. Large Amplitude Ship Motions and Capsizing

The linear response of floating rigid bodies to waves can be described by a coupled system of equations for the six degrees of freedom

$$(\mathbf{M}+\mathbf{A})\,\ddot{\boldsymbol{\xi}}+\mathbf{B}\dot{\boldsymbol{\xi}}+\mathbf{C}\boldsymbol{\xi}=\mathrm{Re}\left(\mathbf{f}_e e^{i\omega t}\right), \tag{1}$$

where $\boldsymbol{\xi}=(\xi,\eta,\zeta,\varphi,\theta,\psi)^T$ represents the vector of generalized coordinates, as defined in Fig. 1. Matrix $\mathbf{M}$ denotes the inertia matrix. The

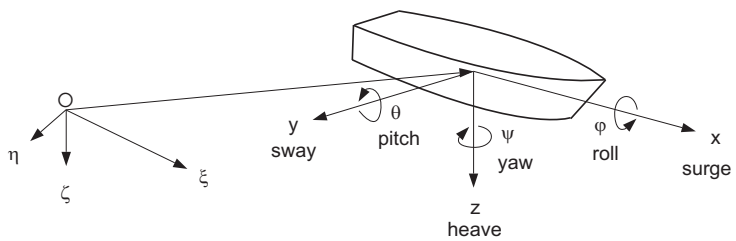

Figure 1. Definition of generalized coordinates

added mass matrix $\mathbf{A}$, the damping matrix $\mathbf{B}$, and the excitation vector $\mathbf{f}_e$ are computed for a given wave frequency, forward velocity, and wave direction applying potential flow theory. The hydrostatic restoring characteristics are described by the matrix $\mathbf{C}$. Assuming harmonic response with the frequency of encounter ω, the vector of the complex Response Amplitude Operator (RAO) yields

$$\mathbf{y}(\omega) = \left[-\omega^2 \left(\mathbf{M} + \mathbf{A}\right) + i\omega\mathbf{B} + \mathbf{C}\right]^{-1} \mathbf{f}_e. \tag{2}$$

For symmetry with respect to the centerline the surge, heave and pitch motions in (1) are decoupled from the sway, roll and yaw motions, so that the linear response for each set of degrees of freedom can be determined independently from each other. This means that the out-of-plane modes sway, roll and yaw motions cannot be excited by linear mechanisms in head or following seas. The roll motion in head and following seas is induced by the nonlinear kinematic coupling of the pitch and heave motion, and primarily by the temporal variation of the righting lever curve in waves.

In order to set up an appropriate model to describe the nonlinear ship roll motion, we follow the linear order of magnitude analysis by Newman (1977) to identify the leading order forces. In waves of wavelengths comparable to the ship length, the hydrostatic forces and the Froude-Krylov forces are of leading order for heave, roll, and pitch modes. Thus, in the first place, it is important to account for the hydrostatic and Froude-Krylov force contributions in the nonlinear model. Further, the forces associated with heave and pitch are at least of one order greater than those associated with the roll motion. We deduce that the nonlinear coupling of heave, roll and pitch motion will affect the roll motion to a higher degree than vice versa, and consider linear heave and pitch behavior as an appropriate assumption.

The nonlinear roll equation of motion will account for nonlinear damping effects and employ the instantaneous righting moment

$$\left[I_{xx} + A_{xx}(\omega_n)\right] \ddot{\varphi} + b_1\dot{\varphi} + b_3\dot{\varphi}^3 = M_r(\zeta, \varphi, \theta, t), \tag{3}$$

where I_{xx} denotes the roll inertia moment of the ship, and $A_{xx}(\omega_n)$ is the hydrodynamic inertia at the roll natural frequency ω_n with

$$\omega_n^2 = g\Delta GM / \left[I_{xx} + A_{xx}(\omega_n) \right], \tag{4}$$

where g denotes the acceleration of gravity, Δ the ship mass, and GM the initial metacentric height. The damping coefficients b_1 and b_3 are obtained by a nonlinear polynomial regression of experimental data for effective damping coefficients (Blume, 1979) for the corresponding block coefficient, beam to draft ratio, and Froude number. The righting moment M_r is determined from the pressure distribution in the incident waves at the actual position of the ship.

Parametric Rolling in Head Seas. We investigate a fast 173 m passenger ferry advancing in head seas at Froude number $F_n = 0.3$ which corresponds to 85% of the service speed. Under these conditions, the encounter frequency in waves of wavelengths comparable to ship length is about twice the natural roll frequency. This two-to-one frequency ratio is assumed to be critical for parametric excitation. The ship responds directly to the wave excitation in the heave and pitch modes and produces an oscillation of the righting lever curve with the frequency of encounter. The RAOs for heave and pitch motions are shown in Fig. 2 and Fig. 3, respectively.

Linear methods generally tend to overstate the response amplitudes at resonance, here at a wave frequency of about 0.5 rad/s for heave and pitch motions. We consider a wave frequency of 0.55 rad/s which corresponds to a wave-to-ship length ratio of 1.2. This frequency is sufficiently far from the resonant wave frequency, so that the results of the linear heave and pitch motion analysis can be employed with confidence.

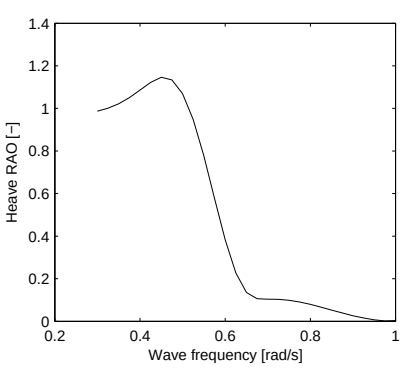

Figure 2. Heave RAO in head seas

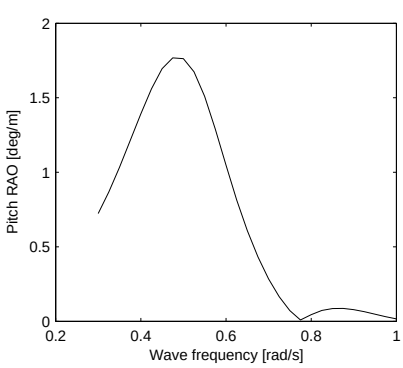

Figure 3. Pitch RAO in head seas

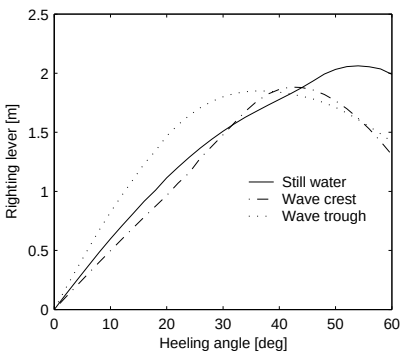

Figure 4. Righting lever curves in head seas, wave height 6 m

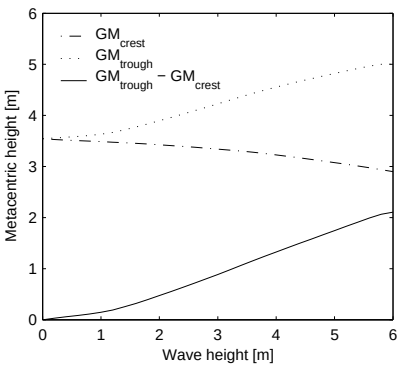

Figure 5. Variation of the initial stability with respect to the wave height

In order to study the variation of the dynamic righting moment, the righting lever curves are computed for still water, wave crest and wave trough condition. Figure 4 compares the dynamic righting lever curves at a wave height of 6 m. In both, crest and trough condition, the maximum righting lever is reduced in comparison to the still water condition.

Further investigations show that the wave crest and trough curves correspond to the limiting curves of the righting lever oscillation. Only for moderate wave heights of up to 1.5 m it can be assumed that the metacentric height GM oscillates about the metacentric height in still water. The dependence of the GM-variation on the wave height is shown in Fig. 5.

For the analytical investigation we approximate the restoring moment curve by a cubic polynomial. The temporal variation of the initial stability in waves is modeled by a harmonically oscillating component. The restoring moment has the form

$$M_r(\zeta, \varphi, \theta, t) = -c(t)\varphi + c_3\varphi^3, \quad \text{with} \tag{5}$$

$$c(t) = g\Delta \left[GM + \frac{\delta_{GM}}{2} \cos(\omega t) \right] = c_1 + c_\delta \cos(\omega t), \tag{6}$$

where δ_{GM} corresponds to the difference between the initial metacentric height in trough and crest condition.

The dynamics of (3) with the restoring moment defined by (5) and (6) can be assessed by the method of multiple scales (Oh et al., 2000). The first approximation yields

$$\varphi(t) = a \cos\left[\frac{1}{2}(\omega t - \gamma) \right], \tag{7}$$

with slowly varying amplitude a and phase γ governed by

$$a' = -\frac{b_1\omega_n^2}{2c_1}a + \frac{3b_3\omega_n^4}{8c_1}a^3 - \frac{c_\delta\omega_n}{2c_1}a\cos\gamma, \tag{8}$$

$$\gamma' = \sigma + \frac{3c_3\omega_n}{4c_1}a^2 - \frac{c_\delta\omega_n}{c_1}\sin\gamma, \tag{9}$$

where the detuning parameter σ is defined by $\omega = 2\omega_n + \sigma$. For the numerical values of all the parameters employed, we refer to Kreuzer and Sichermann (2004). The fixed points of (8) and (9) correspond to stationary solutions of (3). Setting $a' = 0$ and $\gamma' = 0$ yields a nonlinear relation for the excitation and the response amplitude. In combination with the variation of the metacentric height with respect to the wave height, as shown in Fig. 5, the expected roll amplitude can be plotted over the wave height, Fig. 6. It is observed that up to a wave height of 4.8 m, no roll motion is excited. In the interval from 4.8 m to 5.1 m both, zero amplitude and large amplitude motions are possible. Beyond the wave height of 5.1 m there exist only stable motions with large amplitudes.

The investigation of parametrically excited roll motions in harmonic waves represents only a special case of the more general situation in ocean waves. However, essential information on the roll behavior in irregular seas can be obtained from the analysis in regular waves. Numerical simulations of the roll equation (3) show that for an average wave frequency of 0.55 rad/s, large amplitude motions do not occur for significant wave heights smaller than 4.5 m. For greater wave heights, large amplitude motions are observed, and the maximum roll angles correspond to the limiting values found in the analysis of the deterministic case.

While in the deterministic case the choice of initial conditions determines whether the system exhibits large amplitude motions or settles down to the trivial solution, large amplitude motions in irregular waves occur in stochastic patterns. Figure 7 shows the time history of a numerical realization, where the occurrence of large amplitude motions was observed three times within a period of 20 minutes.

Capsizing in Following Seas. We now consider the reference ship at $F_n = 0.3$ in following seas. The frequency of encounter is significantly reduced and the righting lever curve oscillates with a longer period, so that the ship is endangered to capsize on the wave crest before sufficient stability is regained in the wave trough. The reference ship shows very high initial stability ($GM = 3.54$ m) so that the righting lever variation is unlikely to induce capsizing for realistic wave heights. In order to

illustrate the mechanism of capsizing, we reduce the initial metacentric height to 2.0 m corresponding to an increase of the ship's center of gravity by 1.5 m.

In contrast to the scenario of parametrically excited roll motions, where the system behavior is studied in the vicinity of the upright position, the capsizing mechanism has to be investigated at large deviations from the equilibrium position. Therefore, different techniques of analysis have to be introduced. Capsizing is considered to have a mechanical equivalent in the escape problem from a potential well, where the potential is characterized by the righting lever curve. Such problems can be investigated by Melnikov's method, which has already been applied successfully to capsizing analyses of ships in beam seas (Jiang et al., 2000; Spyrou et al., 2002). The roll equation (3) is transformed into the first order system for $\mathbf{x} = (\varphi, \dot{\varphi})^T$

$$\dot{\mathbf{x}} = \mathbf{f}(\mathbf{x}) + \epsilon \mathbf{g}(\mathbf{x}, t), \quad \text{where} \tag{10}$$

$$\mathbf{f}(\mathbf{x}) = \left(\dot{\varphi}, -\alpha_1 \phi + \alpha_3 \varphi^3\right)^T \quad \text{and} \tag{11}$$

$$\epsilon \mathbf{g}(\mathbf{x}, t) = \left(0, -\beta_1 \dot{\varphi} - \beta_3 \dot{\varphi}^3 + \varphi \alpha_\delta \cos(\omega t)\right)^T . \tag{12}$$

Here, new coefficients have been introduced for the sake of clarity. The parameters α_1, α_3, α_δ, and the parameters β_1 and β_3 correspond to the normalized restoring and damping coefficients. The right-hand side of (10) has been split into conservative and non-conservative components. The term (11) accounts for the effect of the average righting lever curve, whereas (12) respects damping and the temporal variation of the righting lever curve. The parameter ϵ emphasizes that (12) is one order of magnitude smaller than (11). Thus, the system will behave approximately like

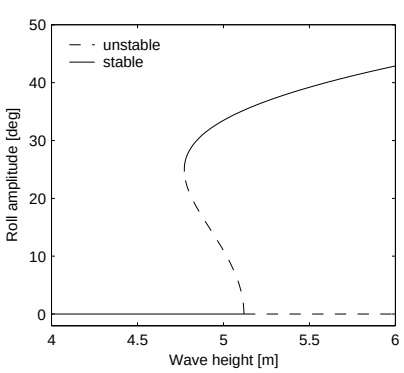

Figure 6. Roll response amplitude in regular head seas

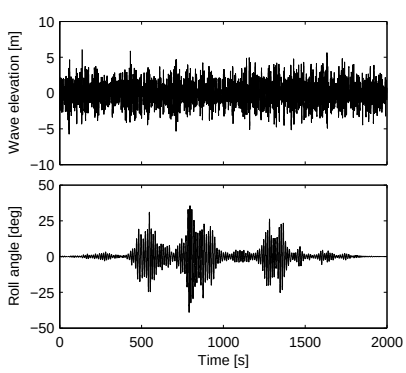

Figure 7. Roll response in irregular seas, significant wave height 5 m

$\dot{\mathbf{x}} = \mathbf{f}(\mathbf{x})$, which shows three fixed points corresponding to the upright position $\varphi = 0$ and to the angles of vanishing stability $\varphi = \pm\varphi_v$ to starboard and port side, respectively. The outer fixed points are connected by heteroclinic trajectories

$$\mathbf{x}_h(\tau) = \pm\sqrt{\frac{\alpha_1}{\alpha_3}}\left[\tanh\left(\sqrt{\frac{\alpha_1}{2}}\tau\right), \sqrt{\frac{\alpha_1}{2}}\cosh^{-2}\left(\sqrt{\frac{\alpha_1}{2}}\tau\right)\right]^T, \qquad (13)$$

which separate the phase space regions of bounded and unbounded motion. The region of bounded motion, enclosed by the heteroclinic trajectories, is referred to as the safe basin. In a conservative system each trajectory corresponds to a constant energy state of the system. Hence, every trajectory starting inside the safe basin cannot cross the basin boundary since this implies increasing the system's energy. The basin boundaries for still water and wave crest condition at a wave height of 8 m are shown in Fig. 8.

Introducing the non-conservative term (12) will alter the system's energy and enable trajectories close to the heteroclinic trajectory to cross the potential barrier. The Melnikov function is here derived from a simple energy viewpoint (Simiu, 2002). The change of energy during motion along the heteroclinic trajectory corresponds to the dissipated energy and to the work performed by the parametric excitation

$$E = -\int_{-\infty}^{\infty}\left(\beta_1\dot{\varphi}_h^2 + \beta_3\dot{\varphi}_h^4\right)\mathrm{d}\tau + \int_{\infty}^{\infty}\varphi_h\dot{\varphi}_h\alpha_\delta\cos\left[\omega(\tau + t_0)\right]\mathrm{d}\tau. \qquad (14)$$

It can be shown that E is equivalent to the Melnikov function $M(t_0)$ of the system (10). For $M(t_0) > 0$, the system's energy is increased, and trajectories close to the basin boundary are likely to escape from the safe domain. The condition $M(t_0) > 0$ is therefore considered as a necessary condition for capsizing. Carrying out the integrations in (14) yields

$$M(t_0) = -k + \alpha_\delta\left|H(\omega)\right|\cos\left[\omega t_0 + \nu(\omega)\right] \quad \text{with} \qquad (15)$$

$$k = \frac{2\sqrt{2}\alpha_1^{3/2}}{3\alpha_3}\beta_1 + \frac{8\sqrt{2}\alpha_1^{7/2}}{35\alpha_3^2}\beta_3, \qquad (16)$$

$$H(\omega) = i\frac{\pi\omega^2}{\alpha_3}\sinh^{-2}\left(\frac{\pi\omega}{\sqrt{2\alpha_1}}\right), \quad \text{and} \qquad (17)$$

$$\nu(\omega) = \arctan\left[\mathrm{Im}H(\omega)/\mathrm{Re}H(\omega)\right]. \qquad (18)$$

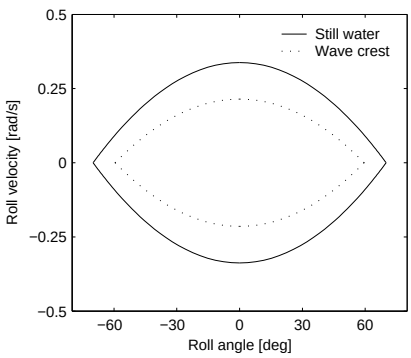

Figure 8. Safe basin boundaries

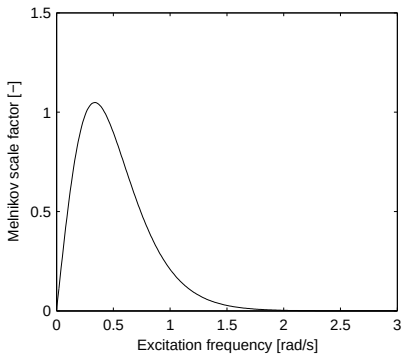

Figure 9. Melnikov scale factor

The Melnikov scale factor $|H(\omega)|$ is shown in Fig. 9. When the excitation is a Gaussian process with the spectral density function $S(\omega)$, the Melnikov function is also Gaussian with mean value $-k$ and spectral density

$$S_M(\omega) = \alpha_\delta^2 |H(\omega)|^2 S(\omega). \tag{19}$$

For a Gaussian Melnikov process the mean time between consecutive zero up-crossings is

$$\tau_{up} = 2\pi \sqrt{\frac{m_0}{m_2}} \exp\left(\frac{k^2}{2m_0}\right), \tag{20}$$

where m_0 and m_2 denote the spectral moments of order zero and two, respectively. Provided that capsizing is a rare event, the probability that there are no zero up-crossings of the Melnikov process during a time interval $T \ll \tau_{up}$ can be approximated by the Poisson distribution with an average waiting time τ_{up}. The probability that there will be at least one zero up-crossing of the Melnikov process in the interval T yields

$$P_{M,T} = 1 - \exp(-T/\tau_{up}). \tag{21}$$

Since $M(t_0) > 0$ is a necessary condition for the escape from the safe basin only, $P_{M,T}$ yields an upper bound for the probability that capsizing occurs within the time interval T. For the specific case of our reference ship and the observation time $T = 1\,\mathrm{h}$, we observe that the upper bound for the capsizing probability starts to increase strongly at a significant wave height of 7.5 m. However, arbitrary choice of the time interval T and of a tolerable capsizing probability will produce distinct limiting wave heights. Nevertheless, the quantitative comparison of different designs is possible, when the considered time interval and the threshold probability are held constant.

3. Mooring Line Dynamics

The mooring lines of ocean engineering systems can spread out over many kilometers. Typically, the lines consist of anchors, heavy chains and nylon ropes or steel cables which are attached to the floating object. A displacement of the attachment point with respect to the equilibrium position causes lowering or lifting of the heavy chain links from the ground and thus results in a restoring force. The force characteristics of this system shows a significantly nonlinear behavior: as the displacement of the vessel increases, the catenary system shows stiffening of the restoring forces. The fluid forces on the transparent mooring lines are obtained from the modified Morison's equation, which gives the incremental normal force $\mathrm{d}F_n$ on a mooring line segment of length $\mathrm{d}s$

$$\mathrm{d}F_n = \left(\rho \frac{\pi D^2}{4} \frac{\partial v_n}{\partial t} + C_a \rho \frac{\pi D^2}{4} \frac{\partial u_{rn}}{\partial t} + C_d \frac{\rho D}{2} |u_{rn}| u_{rn} \right) \mathrm{d}s \qquad (22)$$

with the density of the fluid ρ, the line diameter D, the normalized acceleration of the fluid $\partial v_n/\partial t$, the added mass coefficient C_a, the relative normalized acceleration between the fluid and the structure $\partial u_{rn}/\partial t$, the damping coefficient C_d, and the normalized relative velocity between fluid and structure u_{rn}. Considering the dynamics of mooring lines as a multibody system leads to a large set of differential equations with hundreds of degrees of freedom. Dividing the catenary and the cable into several subsystems as shown in Fig. 10 and including the appropriate boundary conditions for each subsystem can be advantageous for the integration of the equations of motion.

While in general practice only the static forces on the mooring line are considered, the present approach reveals that the dynamical influence must not be neglected, especially in great water depths (Kreuzer and Wilke, 2003). Simulations show that instead of just following the motion of the moored vessel, some parts of the mooring system might rest or even move in the opposite direction as shown in Fig. 11.

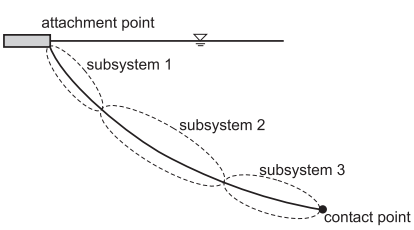

Figure 10. Possible division of subsystems in a catenary mooring system

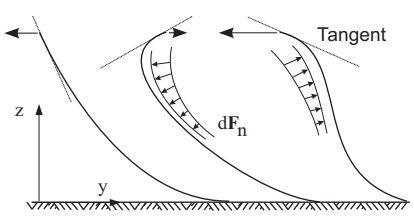

Figure 11. Line motion behavior in great water depths

4. Floating Cranes

One example of a moored multibody system is a floating crane. In addition to the mooring line forces and the fluid-structure interaction, the dynamics is influenced by coupling between the vessel and the swinging load. In our analysis, the forces of the mooring system are simplified by using a polynomial approximation of the static mooring line curve. For the case of in-plane-excitation, the system behavior can be described entirely by the surge, heave, pitch motion and the angle α of the swinging load. This gives a system with four degrees of freedom: $\mathbf{u} = (x, \theta, z, \alpha)^T$. Experiments with floating cranes in a wave tank have shown that such a system may exhibit large amplitude subharmonic motion (Clauss et al., 2000). The subharmonic response was observed to become particularly obvious from the surge motion.

In order to investigate this phenomenon mathematically, two different techniques are applied (Ellermann et al., 2002). The first technique is the multiple scales method, generally applicable to systems with weak nonlinearity. After the order of magnitude analysis and scaling of the different parameters in the equations of motion and the relation between the forcing and the resonance frequencies of the system, we obtain an analytical approximation for the solution. The advantage of this procedure is that it can easily be evaluated for any set of parameters. Figure 12 gives an example of solutions obtained by the multiple scales method. The solid curves indicate the first and the second primary resonance. The shaded areas give the range of the subharmonic P2 (period 2) motion and the dotted curve shows the amplitude of the subharmonic P3 solution.

The second technique, the numerical bifurcation analysis based on a path-following method is applied to give a more precise solution for

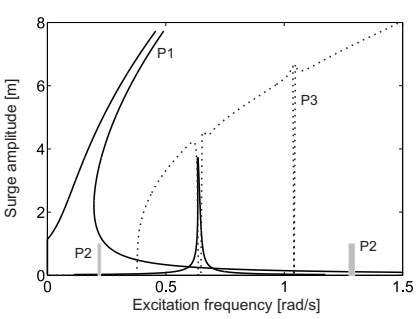

Figure 12. Surge amplitudes by multiple scales analysis

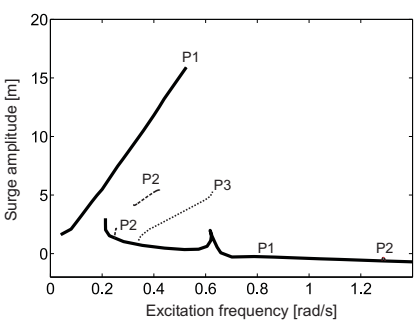

Figure 13. Surges amplitudes by path following

the individual motions and the position of the bifurcation points. Figure 13 shows an example for a numerically determined bifurcation diagram. The parameters correspond to those used in Fig. 12. The bifurcation diagram clearly shows the same two peaks for the first two primary resonances; it gives the P2 motion at the frequencies predicted by the multiple scales method and it also reveals the strong bending of the curve for the P3 motion. The difficulty when applying the path-following technique is that isolated solutions such as the P2 motion at 0.35 rad/s cannot be found directly. Only those solutions which result from a bifurcation can be traced systematically. By using different free parameters in the bifurcation analysis and possibly following periodic solutions beyond the range of validity of the model, some of these different solutions can be found.

5. Conclusions

We have explored the nonlinear dynamics of ships, mooring lines, and floating cranes. The mathematical models of these and other ocean engineering systems are often of high dimensions, especially when the flow problem has to be solved explicitly. In order to promote the understanding of the rather complex dynamic nature, we have focused on the study of model equations with only few degrees of freedom. The analytical investigation of extreme ship motions has been helpful to identify the critical parameters detrimental to the seakeeping behavior of ships in regular and irregular seas.

The accuracy of the approximate models, however, has to be verified with respect to the solutions of full-order models. An example of a sophisticated high-dimensional model was presented by the modeling of mooring line dynamics. The analysis of subharmonic floating crane response has demonstrated how the combination of analytical and numerical techniques can be employed successfully. Further demand of research is identified for the investigation of the nonlinear dynamic behavior of complex systems with random excitation.

References

Blume, P. (1979). Experimentelle Bestimmung von Koeffizienten der wirksamen Rolldaempfung and ihre Anwendung zur Abschaetzung extremer Rollwinkel. *Schiffstechnik*, 26:3–23.

Clauss, G., Vannahme, M., Ellermann, K., and Kreuzer, E. (2000). Subharmonic oscillations of moored floating cranes. In *Proc. of the Offshore Technology Conference*, Houston, TX, 429–436.

Ellermann, K., Kreuzer, E., and Markiewicz, M. (2002). Nonlinear dynamics of floating cranes. *Nonlinear Dyanmics*, 27:107–183.

IMO (2002). *Code on Intact Stability for all Types of Ships Covered by IMO Instruments*. International Maritime Organization, London.

Jiang, C., Troesch, A. W., and Shaw, S. W. (2000). Capsize criteria for ship models with memory-dependent hydrodynamics and random excitation. *Phil. Trans. R. Soc. Lond. A*, 358:1761–1791.

Kreuzer, E. and Sichermann, W. (2004). Investigation of large amplitude roll motions and capsizing. In *Proc. of the 9th International Symposium on Practical Design of Ships and other Floating Structures*, Luebeck-Travemuende, Germany.

Kreuzer, E. and Wilke, U. (2003). Dynamics of mooring systems in ocean engineering. *Archive of Applied Mechanics*, 73:270–281.

Newman, J. N. (1977). *Marine Hydrodynamics*. The MIT Press, Cambridge, MA.

Oh, I. G., Nayfeh, A. H., and Mook, D. T. (2000). A theoretical and experimantal investigation of indirectly excited roll motion in ships. *Phil. Trans. R. Soc. Lond. A*, 358:1853–1881.

Simiu, E. (2002). *Chaotic Transitions in Deterministic and Stochastic Dynamical Systems*. Princeton University Press, Princeton, NJ.

Spyrou, K. J., Cotton, B., and Gurd, B. (2002). Analytical expressions of capsize boundary for a ship with roll bias in beam waves. *Journal of Ship Research*, 46:167–174.

Spyrou, K. J. and Thompson, J. M. T. (eds.) (2000). The nonlinear dynamics of ship motions. *Phil. Trans. R. Soc. Lond. A (Theme Issue)*, 358:1731–1981.